The Astrophysical Journal, 640:L155–L158, 2006 April 1

ATTENUATION OF VERY HIGH ENERGY GAMMA RAYS BY THE MILKY WAY INTERSTELLAR RADIATION FIELD

Igor V. Moskalenko[1]
Hansen Experimental Physics Laboratory, Stanford University, Stanford, CA 94305-4085; imos@stanford.edu
Troy A. Porter
Department of Physics and Astronomy, Louisiana State University, 202 Nicholson Hall, Baton Rouge, LA 70803-4001; tporter@lsu.edu
and
Andrew W. Strong
Max-Planck-Institut für extraterrestrische Physik, Postfach 1312, D-85741 Garching, Germany; aws@mpe.mpg.de
Received 2005 November 2; accepted 2006 February 17; published 2006 March 7

ABSTRACT

The attenuation of very high energy γ-rays by pair production on the Galactic interstellar radiation field has long been thought of as negligible. However, a new calculation of the interstellar radiation field consistent with multiwavelength observations by the DIRBE and FIRAS instruments indicates that the energy density of the Galactic interstellar radiation field is higher, particularly in the Galactic center, than previously thought. We have made a calculation of the attenuation of very high energy γ-rays in the Galaxy, using this new interstellar radiation field, that takes into account its nonuniform spatial and angular distributions. We find that the maximum attenuation occurs around 100 TeV at the level of about 25% for sources located at the Galactic center and is important for both Galactic and extragalactic sources.

Subject headings: Galaxy: general — gamma rays: observations — gamma rays: theory — radiation mechanisms: general — radiative transfer

Online material: color figure

1. INTRODUCTION

The attenuation of very high energy (VHE) γ-rays by pair production on the Galactic interstellar radiation field (ISRF) has previously been considered to be negligible (Nikishov 1962; Protheroe 1986). The main contribution is thought to come from pair production on the cosmic microwave background (CMB), where the effective threshold for attenuation is ~100 TeV and a maximum is reached at about 2000 TeV, currently accessible only by means of air-shower experiments. The Galactic ISRF photons are more energetic, so that the effective threshold is lower (~100 GeV) and the attenuation increases slowly to a maximum around 100 TeV. This covers the energy range of present-day imaging atmospheric Cerenkov telescopes, such as the High Energy Stereoscopic System (HESS). A rough estimate of the attenuation of VHE γ-rays coming from the Galactic center (GC), which uses a new ISRF (Porter & Strong 2005) but assumes an isotropic angular distribution for the ISRF, shows that the effect is observable (Zhang et al. 2005). Given the essential anisotropy of the Galactic ISRF, with most of the photons going outward from the inner Galaxy, the effect depends on the position of the source of VHE photons and its orientation relative to the observer in the Galactic plane. Here we calculate the attenuation of VHE γ-rays due to pair production with the Galactic photon field using the total ISRF over the entire Galaxy on a fine spatial grid that takes into account the nonuniform spatial and anisotropic angular distribution of background photons.

2. INTERSTELLAR RADIATION FIELD

The essential ingredients to calculate the Galactic ISRF are a model for the distribution of stars in the Galaxy, a model for the dust distribution and properties, and a treatment of scattering, absorption, and subsequent reemission of the stellar light by the dust. We briefly describe our ISRF calculation, which is a further development of the work reported in Porter & Strong (2005); full details will be given in a forthcoming paper (T. A. Porter & A. W. Strong 2006, in preparation).

Our stellar model assumes a type classification based on that used in the SKY model of Wainscoat et al. (1992). It includes 87 stellar classes encompassing main-sequence stars, asymptotic giant branch (AGB) stars, and exotics. For each stellar type, there is a local star number density, scale height above the plane, fraction of local number density in each of several discrete spatial components, and spectrum in standard photometric filters. The stars are distributed in seven geometric components: thin and thick disk, halo, bulge, bar, ring, and spiral arms. Spectra for normal stars are taken from the synthetic spectral library of Girardi et al. (2002). Spectra for AGB stars and exotics are as given in the SKY model.

We assume a dust model including graphite, polycyclic aromatic hydrocarbons (PAHs), and silicate. Dust grains in the model are spherical and the absorption and scattering efficiencies for graphite, PAHs, and silicate grains are taken from Li & Draine (2001). The grain model abundance and size distribution are taken from Weingartner & Draine (2001; their best-fit Milky Way model), and a purely neutral interstellar medium is assumed. We consider only coherent scattering, and a Henyey-Greenstein angular distribution function (Henyey & Greenstein 1941) is used in the scattering calculation. The stochastic heating of grains smaller than ~0.1 μm is treated using the "thermal continuous" approach of Draine & Li (2001); we calculate the equilibrium heating of larger dust grains by balancing absorption with reemission as described by Li & Draine (2001).

Dust is assumed to follow the Galactic gas distribution. We use the gas model for neutral and molecular hydrogen given in Moskalenko et al. (2002). The radial variation in the Galactic

[1] Also Kavli Institute for Particle Astrophysics and Cosmology, Stanford University, Stanford, CA 94309.

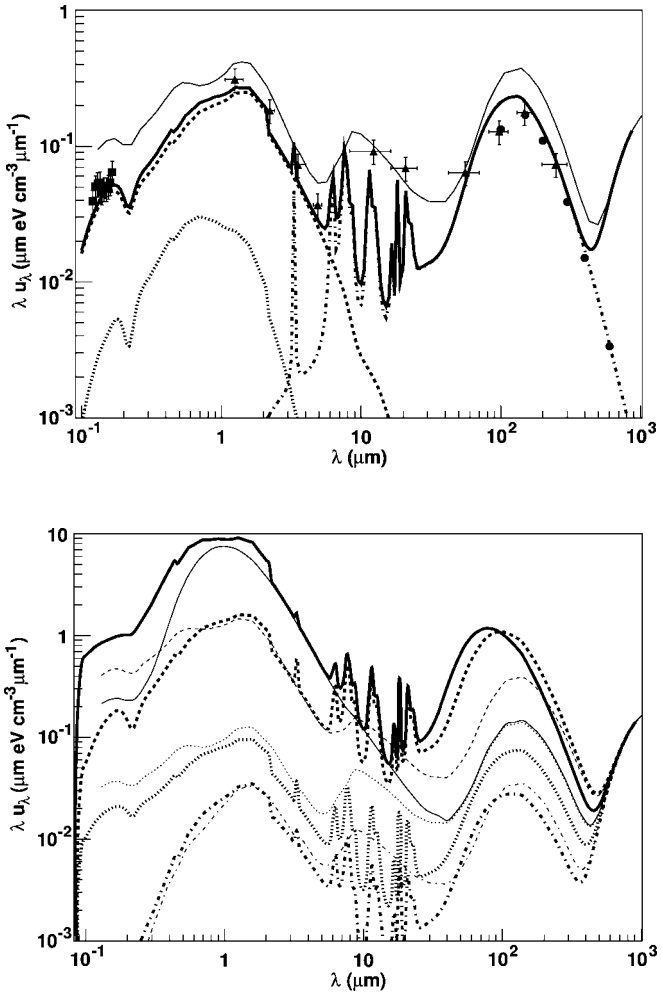

FIG. 1.—Interstellar radiation field energy density. *Top*: Local interstellar radiation field. *Thick solid line*, total radiation field including CMB; *thick dashed line*, contribution by stars; *thick dotted line*, scattered light; *thick dot-dashed line*, infrared; *thin solid line*, local ISRF from Strong et al. (2000). Data: *Squares*, *Apollo* (Henry et al. 1980); *triangles*, DIRBE (Arendt et al. 1998); *circles*, FIRAS (Finkbeiner et al. 1999). *Bottom*: Interstellar total radiation field radial variation. *Solid lines*, $(R, z) = (0 \text{ kpc}, 0 \text{ kpc})$; *dashed lines*, $(R, z) = (4 \text{ kpc}, 0 \text{ kpc})$; *dotted lines*, $(R, z) = (12 \text{ kpc}, 0 \text{ kpc})$; *dash-dotted lines*, $(R, z) = (16 \text{ kpc}, 0 \text{ kpc})$. Thick lines are for our ISRF; thin lines are for the ISRF of Strong et al. (2000).

metallicity gradient is taken to be 0.07 dex kpc^{-1} (Strong et al. 2004 and references therein).

A cylindrical geometry is adopted for the radiation-field calculation. Our calculations are simplified by assuming symmetry in azimuth and about the Galactic plane. The maximum radial extent is taken to be $R_{\max} = 20$ kpc. The maximum height above the Galactic plane is taken to be $z_{\max} = 5$ kpc. The Sun is located at $R_S = 8.5$ kpc from the GC. The Galaxy is divided into elements of equal volume, and the total radiation field is calculated for each.

The radiation field from stellar and scattered light is obtained using a modified form of the so-called partial-intensity method (Baes & Dejonghe 2001). Henceforth, we will refer to the total stellar and scattered light as the "optical" radiation field. The infrared radiation field is obtained by using the optical radiation field to calculate the dust emissivity for stochastic and equilibrium heating. The dust emission is integrated to obtain the infrared radiation field throughout the Galaxy.

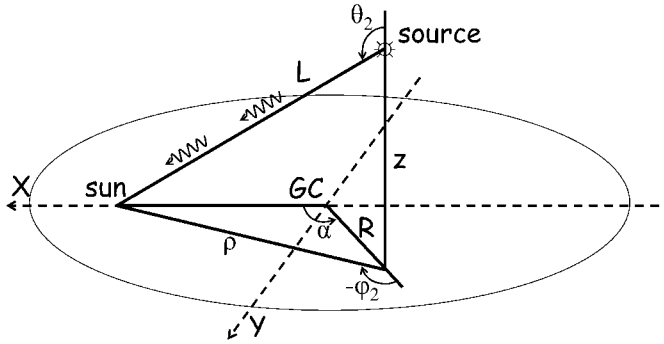

FIG. 2.—Angles involved in the calculation: (R, z, α), Galactocentric coordinates of the source of VHE photons; (θ_2, ϕ_2), angles of the VHE photon. GC marks the Galactic center, and the observer's position is marked by "sun."

Figure 1 (*top*) shows our calculated local ISRF including the CMB; also shown in the figure is the local ISRF calculated by Strong et al. (2000). The agreement of our computed ISRF with the data is generally good. We note that our new ISRF provides an improved fit to the observations around 100 μm compared with the earlier model of Strong et al. (2000). This is particularly important for our optical depth calculation, since the majority of the attenuation is on these more numerous, less energetic photons of the ISRF.

The bottom panel of Figure 1 shows the radial variation in the Galactic plane of our ISRF (*thick lines*) together with that of Strong et al. (2000; *thin lines*). Toward the inner Galaxy, our ISRF predicts a significantly higher energy density than previously described, particularly for the infrared component. This arises because of the coupling between the optical radiation field and the infrared emission: in our calculation, the optical radiation field is used as direct input to the dust heating calculation, which was not done in previous work. The intense optical radiation field toward the inner Galaxy heats the dust to warmer temperatures, increasing the emission in the infrared. Even though the optical emission does not cause a direct enhancement to the attenuation at GeV to TeV energies—the energy of these photons is typically a few eV, lowering the threshold, but their number density is too low to provide significant absorption—it is essential to calculate this component of the ISRF to obtain the correct emission and angular distribution for the infrared. Further discussion of the new ISRF is deferred to a forthcoming paper (T. A. Porter & A. W. Strong 2006, in preparation).

3. CALCULATIONS

The optical depth for VHE γ-rays is given by the general formula

$$\tau_{\gamma\gamma}(E) = \int_L dx \int d\epsilon \int d\Omega_1 \frac{dN(\epsilon, \Omega_1, \boldsymbol{x})}{d\epsilon\, d\Omega_1} \sigma_{\gamma\gamma}(\epsilon_c)(1 - \cos\theta), \tag{1}$$

where $dN(\epsilon, \Omega_1, \boldsymbol{x})/d\epsilon\, d\Omega_1$ is the differential number density of background photons at the point $\boldsymbol{x}$, ϵ is the background photon energy, $d\Omega_1 = d\cos\theta_1\, d\phi_1$ is a solid angle, $\sigma_{\gamma\gamma}$ is the total cross section for the pair production process $\gamma\gamma \rightarrow e^+e^-$ (Jauch & Rohrlich 1980), $\epsilon_c = [\frac{1}{2}\epsilon E(1 - \cos\theta)]^{1/2}$ is the center-of-momentum system energy of a photon, and θ is the angle between the momenta of the two photons in the observer's

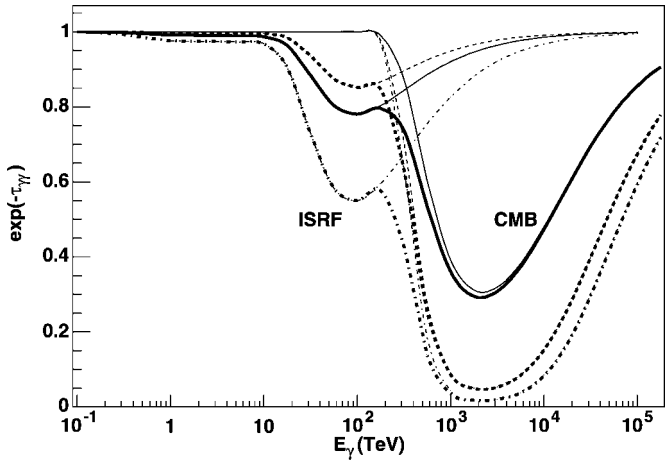

FIG. 3.—Transmittance of VHE γ-rays as a function of γ-ray energy. *Solid lines*, $(R, z, \alpha) = (0 \text{ kpc}, 0 \text{ kpc}, 0°)$ ($L = 8.5$ kpc); *dashed lines*, $(R, z, \alpha) = (20 \text{ kpc}, 0 \text{ kpc}, 90°)$ ($L = 21.8$ kpc); *dash-dotted lines*, $(R, z, \alpha) = (20 \text{ kpc}, 0 \text{ kpc}, 180°)$ ($L = 28.5$ kpc). Thick lines give the total transmittance curve including the ISRF and CMB. The leftmost thin lines give the transmittance for the ISRF only, and the rightmost thin lines that for the CMB only.

frame. The integral over $\boldsymbol{x}$ should be taken along the path of the γ-rays from the source to the observer.

The ISRF is cylindrically symmetric so that the photon angular distribution depends on R and z only. In Figure 2, we illustrate the Galactocentric coordinate system (R, z, α). To calculate $\cos\theta$, the polar and azimuthal angles of the VHE photon, θ_2 and ϕ_2, are derived:

$$\rho^2 = R^2 + R_S^2 - 2RR_S\cos\alpha,$$
$$\sin\theta_2 = \rho(\rho^2 + z^2)^{-1/2}, \quad \cos\theta_2 = -(1 - \sin^2\theta_2)^{1/2},$$
$$\sin\phi_2 = -\frac{R_S\sin\alpha}{\rho}, \quad \cos\phi_2 = -\frac{\rho^2 + R^2 - R_S^2}{2R\rho},$$
$$\cos\theta = \cos\theta_1\cos\theta_2 + \sin\theta_1\sin\theta_2\cos(\phi_1 - \phi_2), \tag{2}$$

where R_S is the Galactocentric radius of the Sun. The integration of equation (1) is done numerically.

For the calculation of the optical depth in the CMB field, we use the formula

$$\tau_{\gamma\gamma}^{\rm CMB}(E) = -\frac{4kT}{(\hbar c)^3\pi^2E^2} \times \int_L dx \int_{m_ec^2}^{\infty} d\epsilon_c\,\epsilon_c^3\sigma_{\gamma\gamma}(\epsilon_c)\log(1 - e^{-\epsilon_c^2/EkT}), \tag{3}$$

where kT is the CMB temperature and m_ec^2 is the electron rest mass.

4. RESULTS

Figure 3 shows the attenuation for selected positions (R, z, α) as a function of incident γ-ray energy. For sources located at the GC, the attenuation is ~12% at 30 TeV and ~23% at 100 TeV. In Table 1, we give our optical depth results for selected values of R and z for $\alpha = 0°$, 90°, and 180° at 30 and 100 TeV without contribution by the CMB. The attenuation is strongest for VHE γ-ray sources located toward the inner Galaxy and on its far side.

TABLE 1

OPTICAL DEPTH $\tau_{\gamma\gamma}$ AT 30 AND 100 TeV

R (kpc)	30 TeV			100 TeV		
	$\alpha = 0°$	$\alpha = 90°$	$\alpha = 180°$	$\alpha = 0°$	$\alpha = 90°$	$\alpha = 180°$
$z = 0$ kpc:						
0	0.12	...	...	0.25	...	...
5	0.01	0.15	0.22	0.05	0.32	0.41
10	0.01	0.08	0.28	0.02	0.21	0.54
15	0.02	0.07	0.31	0.05	0.18	0.58
20	0.03	0.07	0.32	0.06	0.16	0.60
$z = 5$ kpc:						
0	0.03	...	...	0.09	...	...
5	0.01	0.04	0.06	0.05	0.10	0.15
10	0.02	0.05	0.09	0.04	0.12	0.21
15	0.03	0.05	0.12	0.05	0.13	0.26
20	0.03	0.06	0.14	0.06	0.13	0.29

To illustrate the effect of the anisotropic radiation field on the attenuation calculation, in Figure 4 we show as a function of position the ratio of the optical depths $\tau_{\gamma\gamma}/\tau_{\gamma\gamma}^{\rm iso}$, where $\tau_{\gamma\gamma}$ is calculated using the full angular distribution of the ISRF and $\tau_{\gamma\gamma}^{\rm iso}$ is calculated assuming an isotropic distribution, for a source

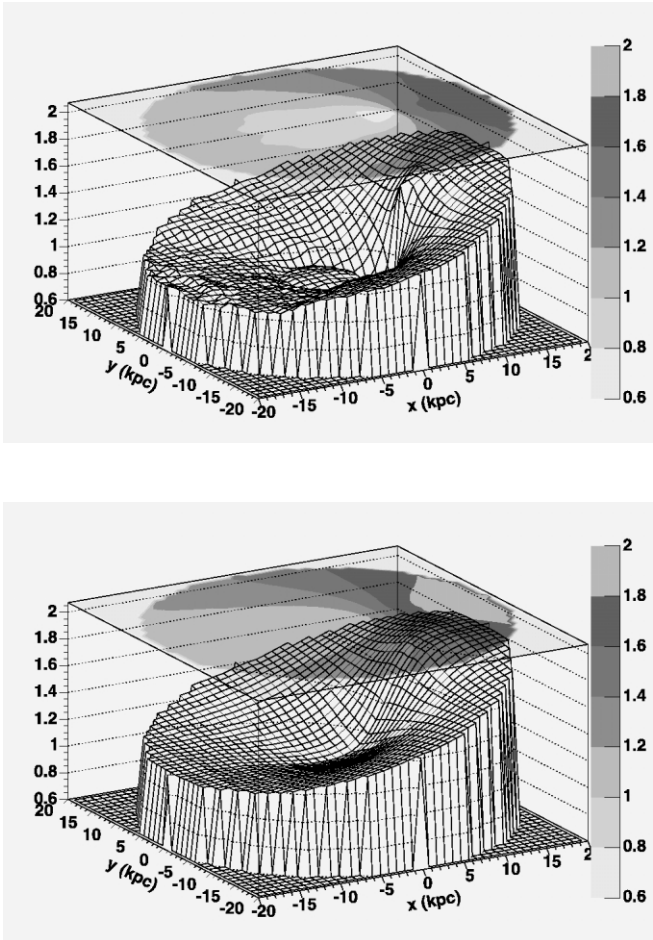

FIG. 4.—Effect of anisotropic ISRF on optical depth calculation at 100 TeV. Shown is the ratio of the optical depths $\tau_{\gamma\gamma}/\tau_{\gamma\gamma}^{\rm iso}$ as a function of position (x, y) for a source located at $z = 0$ kpc (*top*) and $z = 5$ kpc (*bottom*). The solar system is located at $(x, y) = (8.5 \text{ kpc}, 0 \text{ kpc})$, exactly where the optical depth ratio rises sharply. [*See the electronic edition of the Journal for a color version of this figure.*]

located at $z = 0$ kpc (*top*) and $z = 5$ kpc (*bottom*) emitting 100 TeV γ-rays. The variation of $\tau_{\gamma\gamma}/\tau_{\gamma\gamma}^{\rm iso}$ over the Galaxy as seen from Earth is nontrivial. For sources located in the Galactic plane between the GC and solar system, the ratio is less than 1, since the majority of the ISRF photons are coming from the GC direction, $\cos\theta \rightarrow 1$ in equation (1), and the interactions are mainly following, leading to a lower pair production probability when the ISRF angular distribution is taken into account. The reverse situation, $\tau_{\gamma\gamma}/\tau_{\gamma\gamma}^{\rm iso} > 1$, occurs for γ-rays interacting with the ISRF in the outer Galaxy, where the majority of interactions are now head-on, $\cos\theta \rightarrow -1$ in equation (1). For sources located beyond the GC, the ratio is $\sim$1. The interpretation of this case is straightforward: γ-rays emitted on the far side of the Galaxy toward the solar system have mainly head-on absorption interactions until they reach the GC, whereupon the interactions become mainly following. The isotropic case averages the angular distribution and therefore leads to $\tau_{\gamma\gamma}/\tau_{\gamma\gamma}^{\rm iso} \sim 1$. We note that the optical depth ratio increases monotonically with z and is a result of the progressively more head-on nature of the γ-ray absorption interactions for sources located at larger distances from the plane.

Our results show that the attenuation of VHE γ-rays by the Galactic radiation field may be marginally observable by the HESS instrument, which has an effective sensitivity up to several tens of TeV (Aharonian et al. 2006). The attenuation of VHE γ-rays from the sources on the Galaxy's far side will essentially steepen their spectra above $\sim$10 TeV. In any case, correction of source spectra for absorption is required. Interestingly, observations by future high-energy experiments of the steepening of the spectra of Galactic sources in the GC region and beyond may serve as a probe of the Galactic ISRF.

I. V. M. acknowledges partial support from a NASA Astronomy and Physics Research and Analysis Program (APRA) grant. T. A. P. acknowledges partial support from the US Department of Energy.

REFERENCES

Aharonian, F., et al. 2006, ApJ, 636, 777
Arendt, R. G., et al. 1998, ApJ, 508, 74
Baes, M., & Dejonghe, H. 2001, MNRAS, 326, 722
Draine, B. T., & Li, A. 2001, ApJ, 551, 807
Finkbeiner, D., Davis, M., & Schlegel, D. J. 1999, ApJ, 524, 867
Girardi, L., Bertelli, G., Bressan, A., Chiosi, C., Groenewegen, M. A. T., Marigo, P., Salasnich, B., & Weiss, A. 2002, A&A, 391, 195
Henry, R. C., Anderson, R. C., & Fastie, W. G. 1980, ApJ, 239, 859
Henyey, L. G., & Greenstein, J. L. 1941, ApJ, 93, 70
Jauch, J. M., & Rohrlich, F. 1980, Theory of Photons and Electrons (2nd ed.; New York: Springer)
Li, A., & Draine, B. T. 2001, ApJ, 554, 778
Moskalenko, I. V., Strong, A. W., Ormes, J. F., & Potgieter, M. S. 2002, ApJ, 565, 280
Nikishov, A. I. 1962, Soviet Phys.–JETP, 14, 393
Porter, T. A., & Strong, A. W. 2005, Proc. 29th Int. Cosmic Ray Conf. (Pune), 4, 77
Protheroe, R. J. 1986, MNRAS, 221, 769
Strong, A. W., Moskalenko, I. V., & Reimer, O. 2000, ApJ, 537, 763
Strong, A. W., Moskalenko, I. V., Reimer, O., Digel, S., & Diehl, R. 2004, A&A, 422, L47
Wainscoat, R. J., Cohen, M., Volk, K., Walker, H. J., & Schwartz, D. E. 1992, ApJS, 83, 111
Weingartner, J. C., & Draine, B. T. 2001, ApJ, 548, 296
Zhang, J.-L., Bi, X.-J., & Hu, H.-B. 2005, preprint (astro-ph/0508236)